International Journal of Astrobiology

cambridge.org/ija

Research Article

Cite this article: Zaia DAM, Coutinho MA, Mosca DH, da Costa ACS, Urbano A (2020). Study of the formation of ferrihydrite under prebiotic chemistry conditions: artificial seawater 4.0 Gy and ammonium thiocyanate. *International Journal of Astrobiology* **19**, 462–473. https://doi.org/10.1017/S1473550420000245

Received: 24 February 2020
Revised: 12 August 2020
Accepted: 14 August 2020
First published online: 15 September 2020

Key words:
Ammonium thiocyanate; iron oxides; origin of life; XPS

Author for correspondence:
Dimas A. M. Zaia,
E-mail: damzaia@uel.br

CAMBRIDGE UNIVERSITY PRESS

Study of the formation of ferrihydrite under prebiotic chemistry conditions: artificial seawater 4.0 Gy and ammonium thiocyanate

Dimas A. M. Zaia[1], Murilo A. Coutinho[1], Dante H Mosca[2], Antônio C. S. da Costa[3] and Alexandre Urbano[4]

[1]Laboratório de Química Prebiótica-LQP, Departamento de Química, Universidade Estadual de Londrina, CEP 86.057-970 Londrina, PR, Brazil; [2]Departamento de Física, Universidade Federal do Paraná, Centro Politécnico, Curitiba 81531-980, Paraná; [3]Departamento de Agronomia-CCA, Universidade Estadual de Maringá, Maringá 87020-900, PR, Brazil and [4]Departamento de Física-CCE, Universidade Estadual de Londrina, CEP 86057-970 Londrina, PR, Brazil

Abstract

Among the several steps involved in molecular evolution, molecular preconcentration is the first and most important. If the molecules are not preconcentrated the other steps of molecular evolution cannot occur. There are several ways to preconcentrate molecules: sorption, wetting/drying cycles, freezing/sublimation and sorption/precipitation with minerals. In the present work, the effect of NH_4SCN and artificial seawater 4.0 Gy on the synthesis of ferrihydrite was studied. It should be noted that thiocyanate could play the same role as that of CN^- in the Strecker reaction. Unlike today's seawater that has high Na^+ and Cl^- concentrations, the seawater used in this work has high Mg^{2+}, Ca^{2+} and SO_4^{2-} concentrations. Two results stand out, first SCN^- and NH_4^+ were preconcentrated by sorption/precipitation in some syntheses and second, in some experiments, a mixture of goethite, hematite and magnetite was obtained. The sorption/precipitation of SCN^- is always associated with the synthesis of goethite. This could be an indication that SCN^- interacts with Fe^{3+} through the sulphur group of SCN^-. In addition, the synthesis of magnetite could be an indication that the SCN^- ion oxidized, forming thiocyanogen-$(SCN)_2$ or trithiocyanate ion-$(SCN)_3^-$ and that Fe^{3+} reduced to Fe^{2+}. Besides the sorption/precipitation of SCN^- and NH_4^+, Fourier-transform infrared spectroscopy also showed that sorption/precipitation of SO_4^{2-} and CO_3^{2-} occurred. Ferrihydrite synthesized with artificial seawater presented the highest surface area and pore size. The pH_{pzc} values of the samples were in the range of pH_{pzc} described in the literature. The X-ray photoelectron spectroscopy (XPS) measurements performed show proportions of iron present in different oxidation states, however, the electronic similarities observed in the mixtures of iron oxides and oxy-hydroxides make it difficult to quantify them. Direct comparison between XPS spectra of the Fe2p and O 1s core-levels reveal no significant differences from the effect of artificial seawater 4.0 Gy on the synthesis of ferrihydrite.

Introduction

Iron is the fourth most abundant element in the Earth's crust (~5.1%). It is found in oceans, rivers, lakes, groundwater, rocks and soils, and is an essential element to living organisms (Murad and Fischer, 1988; Cornell and Schwertmann, 2003). There are 16 Fe-oxides/hydroxides/oxide-hydroxides, which we will call iron oxides (Cornell and Schwertmann, 2003). Iron is also found in several primary minerals such as olivine, pyroxenes, biotite, pyrite, marcasite, greigite, mackinawite, jarosite, vivianite, siderite and different clay minerals (Murad and Fischer, 1988; Schwertmann and Fitzpatrick, 1992). It should be noted that most of these minerals could be found in the prebiotic Earth (Hazen *et al.*, 2008).

The concentration of Fe in minerals ranges from 78% in *wüstite (FeO)* to traces in clay minerals (Murad and Fischer, 1988). Fe^{2+} in clay minerals plays several roles such as degradation of pesticides, dichlorination of chlorinated aliphatic and reduction of nitroaromatics (Stucki, 2006). In addition, there are several other uses for clay minerals, however, one of the most outstanding applications is adsorption of metals and organic molecules (Savic *et al.*, 2014). Montmorillonite is a 2:1 clay mineral found in prebiotic Earth (Hazen *et al.*, 2008) and, as montmorillonite has a high surface area and interacts with organic molecules, it is the most widely studied mineral in prebiotic chemistry (Zaia, 2004, 2008; Lambert, 2008). However, the role played by Fe^{2+} present in clay minerals in prebiotic chemistry has not been fully explored and is not yet fully understood. Usually, studies are limited to explaining the adsorption of organic molecules onto clays due to interaction with metals (Lambert, 2008). Fe^{2+} in clay minerals could have the same role as in olivine; i.e., it could be an electron

donator for the synthesis of molecules. Mössbauer spectroscopy studies have shown a decrease in Fe^{2+} content when adenine, cytosine, thymine and uracil were adsorbed onto montmorillonite, suggesting a reaction between the nucleic acid bases and the metal and not just a sorption process (Carneiro et. al., 2011).

Several molecules (haemoglobin, peroxidase, catalase, ferredoxin, cytochrome-C, ferrichrome, enterochelin and ferritin) that participate in the important physiological processes of living beings contain iron (Murad and Fischer, 1988; Curi and Procopio, 2017). In addition, iron deficiency has been associated with several diseases such as neurodegenerative diseases, anaemias, hemophagocytic syndrome and cardiovascular diseases (Curi and Procopio, 2017; Svobodova *et al.*, 2020). Thus, iron plays important roles in today's living beings and is relevant to better comprehend the geochemical cycle of iron. Iron participates in several geochemical processes. Nowadays, the high oxygen concentration in the atmosphere favours the hydrolysis of olivine/fayalite (reaction 1) or pyrite (reaction 2) to form goethite (Schwertmann and Fitzpatrick, 1992), the most conspicuous iron oxide in soils in the present Earth.

$$Fe_2SiO_4 + 0.5\ O_2 + 3H_2O \rightarrow 2\alpha\text{-}FeOOH + Si(OH)_4 \quad (1)$$

$$4FeS_2 + 15O_2 + 10H_2O \rightarrow 4\alpha\text{-}FeOOH + 8H_2SO_4 \quad (2)$$

In aerobic environments, iron oxides such as goethite are very stable. However, at a very acidic pH (pH < 4 - reaction 3) or in anaerobic environments (reaction 4) the iron oxides can be dissolved and reduced, respectively (Schwertmann and Fitzpatrick, 1992).

$$\alpha\text{-}FeOOH + 3H^+ \rightarrow Fe^{3+} + 2H_2O \quad (3)$$

$$4\alpha\text{-}FeOOH + CH_2O + 8H^+ \rightarrow 4Fe^{2+} + CO_2 + 7H_2O \quad (4)$$

Reaction 4 is important in anaerobic environments present in lakes, rivers, swamps and soils (Schwertmann and Fitzpatrick, 1992). Other iron minerals, siderite and vivianite are synthesized in anaerobic environments. In addition, in anaerobic environments, the reduction of sulphate to sulphide by the bacteria desulfovibrio sp. favours the formation of pyrite (Schwertmann and Fitzpatrick, 1992).

Before 2.5 billion years ago the oxygen in the atmosphere was too low (Kasting, 1987; 2009; Shaw, 2016). The main sinks of Fe^{2+} could be inorganic carbon (CO_3^{2-}), dissolved silica (SiO_2) and sulphide (S^{2-}) (Tosca *et al.*, 2019). These three sinks produced siderite ($FeCO_3$), greenalite ($Fe_3Si_2O_5(OH)_4$) and pyrite (FeS_2) (Tosca *et al.*, 2019). It should be noted that before the biological precipitation of silica from the seawater, the amount of dissolved silica in the seas was much higher than today (Siever, 1992). Furthermore, the P_{CO2} was much higher 3.85 billion years ago than today (Kasting, 2009; Shaw, 2016). Another sink for Fe^{2+} is the formation of green rust (Halevy *et al.*, 2017). However, for the oxidation of Fe^{2+} to Fe^{3+} and the formation of green rust the samples require contact with air for 1.5 h (Halevy *et al.*, 2017). The oxidation of Fe^{2+} to Fe^{3+} could be carried out without the use of oxygen, in environments more similar to the prebiotic Earth (Braterman *et al.*, 1983; Liang *et al.*, 2006).

It should be noted that most iron hydroxide-oxides are made up of Fe^{3+} (Cornell and Schwertmann, 2003). However, due to the reduced atmosphere of Earth, most of the iron on Earth was in the form of Fe^{2+} in minerals such as olivine, pyroxene, Fe-Ni metal and FeS (Hazen *et al.*, 2008). However, there are several ways in which iron hydroxide-oxides could be formed under the conditions that existed on prebiotic Earth. Here are a few examples of how this could have happened: (a) serpentinization reaction in hydrothermal environments (reaction5) (Martin *et al.*, 2008),

$$(Mg,\ Fe)_2SiO_4 + H_2O + \text{"C"} \rightarrow Mg_3Si_2O_5(OH)_4 + Fe_3O_4 + H_2 + CH_4 + C_2\text{-}C_5 \quad (5)$$

(b) oxidation of Fe^{2+} into Fe^{3+} by hydrogen peroxide formed in ice through UV radiation (Liang *et al.*, 2006), (c) oxidation of Fe^{2+}into Fe^{3+} through UV radiation, which was one of the major sources of energy on prebiotic Earth (Braterman *et al.*, 1983) and (d) oxidation of Fe^{2+} to Fe^{3+} in temperatures ranging from 300 °C to 350 °C, pressures ranging from 10 MPa to 25 MPa and pH values ranging from 9.5 to 14 (Bassez, 2018). All these environments existed on prebiotic Earth or still exist (Holm and Andersson, 2005; Martin *et al.*, 2008). Thus, in such environments, ferrihydrite could be synthesized and maybe an intermediary for the synthesis of hematite, goethite and lepidocrocite (Rzepa *et al.*, 2016; Bassez, 2018).

In addition to a number of applications in science and technology (Cornell and Schwertmann, 2003), several iron oxides have been used in prebiotic chemistry experiments such as sorption of biomolecules or precursors of biomolecules (Matrajt and Blanot, 2004; Vieira *et al.*, 2011; Shanker *et al.*, 2013; Canhisares-Filho *et al.*, 2015; Farias *et al.*, 2016; Zaia *et al.*, 2020), catalyzation of the formation of biomolecules (Shanker *et al.*, 2011; Bizzarri *et al.*, 2018; Barge *et al.*, 2019) and catalysation of the formation of biopolymers (Matrajt and Blanot, 2004; Shanker *et al.*, 2012; Georgelin *et al.*, 2017).

SCN^- has been found in hydrothermal vents (Dowler and Ingmanson, 1979) and synthesized from reactions between HCN and S_8 (Bartlett and Davis, 1958). NH_4SCN has been synthesized in experiments simulating prebiotic atmospheres containing H_2S (Mukhin L., 1974; Raulin and Toupance, 1977). It should be noted that thiocyanate could play the same role as that of CN^- in the Strecker reaction (Perezgasga *et al.*, 2003; Wagner and Ofial, 2015; Kouznetsov and Galvis, 2018). In addition, thiocyanate could replace toxic cyanide as a CN-source for the synthesis of tertiary amines (Wagner and Ofial, 2015; Kouznetsov and Galvis, 2018). NH_3 has been found in comets and could be produced by the reduction of NO_2^- by Fe^{2+} (Summers, 1999; Shinnaka *et al.*, 2016). Thus, SCN^- and NH_3 were most likely to be found on the prebiotic earth.

Artificial seawater was used in the experiments, with a composition which, unlike modern seawater, has high concentrations of Mg^{2+}, Ca^{2+} and SO_4^{2-} (Zaia, 2012). This artificial seawater probably better resembles the seawater of the oceans of the Earth 4.0 billion years ago. Based on the work of Izawa *et al.* (2010), Zaia (2012) suggested this artificial seawater. Izawa *et al.* (2010) used hot water to extract soluble salts from Tagish Lake meteorites. The authors obtained the following order of cations: $Mg^{2+} > Ca^{2+} >> Na^+ \approx K^{+,}$ and anions: $SO_4^{2-} >> Cl^-$. In the last few years, we have been using this artificial seawater, 4.0 Gy and the results showed that the ion composition of seawater has an effect on the adsorption of nucleic acid bases as well as on

https://doi.org/10.1017/S1473550420000245 Published online by Cambridge University Press

the stability of the minerals (Canhisares-Filho *et al.*, 2015; Anizelli *et al.*, 2016*a*,*b*; Carneiro *et al.*, 2017; Villafañe-Barajas *et al.*, 2018; Zaia *et al.*, 2018).

Since iron is one of the most abundant elements in the crust of the Earth, we can suppose that it may have had an important role in the origin of life on Earth. The main goals of this work were to synthesize ferrihydrite under prebiotic chemistry conditions and analyse the products of the reaction. Ferrihydrite was synthesized in the presence of NH_4SCN and artificial seawater 4.0 Gy. The products of the reaction were analysed using Fourier-transform infrared (FT-IR) spectroscopy, X-ray photoelectron spectroscopy and X-Ray Diffractometry. In addition, surface area, pore volume, pore size and pH at the point of zero charge were measured.

Materials and methods

Materials

All the reagents were of analytical grade P.A.

Seawater 4.0 Gy

The following substances were weighed and dissolved with ultrapure water until reaching a solution of 1.0 L: Na_2SO_4 (0.2710 g), $MgCl_2.6H_2O$ (0.5000 g), $CaCl_2$ $2H_2O$ (2.5008 g), KBr (0.0502 g), K_2SO_4 (0.4006 g) and $MgSO_4$ (15.000 g) (Zaia, 2012).

Syntheses

The syntheses were performed using distilled water or artificial seawater 4.0 Gy. Ammonium thiocyanate was added in two different ways: (a) in the beaker together with ferric nitrate and (b) in the burette together with potassium hydroxide. When ammonium thiocyanate was added in the beaker together with ferric nitrate, we analysed the effect of high ammonium thiocyanate concentration on the products of the synthesis. When ammonium thiocyanate was added in the burette together with potassium hydroxide, we analysed the effect of low ammonium thiocyanate concentration on the products of the synthesis.

2.1.2.1. Syntheses of ferrihydrite-6-lines (Fh-6) in ultrapure water and in artificial seawater 4.0 (Fh-SW-4.0). Ferrihydrite was synthesized according to the method described by Cornell and Schwertmann (2003). For Fh-6 synthesis, the reagents were dissolved in ultrapure water and for Fh-SW-4.0 synthesis in artificial seawater 4.0. Initially, 100 mL of a solution of iron nitrate ($Fe(NO_3)_3.9H_2O$; 0.20 mol L^{-1}) was added to a plastic box. This solution was kept at a temperature of 75° C with constant stirring. Subsequently, approximately 66 mL of a solution of KOH 1.0 mol L^{-1} was added. The addition of the potassium hydroxide was performed slowly at a steady flow, during 1 h, until reaching a pH of 7.5. The material was filtered in a vacuum system and washed with ultrapure water 3.0 L in order to remove nitrate excess. The material was lyophilized and the ferrihydrite was characterized by X-Ray diffraction and FTIR. All syntheses were performed in duplicate.

2.1.2.2. Syntheses of ferrihydrite in ultrapure water (Fh-DW-NH_4SCN-1) and in artificial seawater 4.0 (Fh-SW-NH_4SCN-1): ammonium thiocyanate (NH_4SCN) plus ferric nitrate hydrate [$Fe(NO_3)_3 9H_2O$] together in the beaker. For Fh-DW-NH_4SCN-1 synthesis, the reagents were dissolved in ultrapure water and for Fh-SW-NH_4SCN-1 synthesis in artificial seawater 4.0. Synthesis occurred under the same conditions as in 2.1.2, with only one change: NH_4SCN and $Fe(NO_3)_3 9H_2O$ were added to the beaker at the ratio Fe^{3+} 1 mol:1 mol NH_4SCN. After the synthesis, the same treatments were performed as in the 2.1.2. synthesis.

2.1.2.3. Syntheses of ferrihydrite in ultrapure water (Fh-DW-NH_4SCN-2) and in artificial seawater 4.0 (Fh-SW-NH_4SCN-2): ammonium thiocyanate (NH_4SCN) plus potassium hydroxide (KOH) together in the burette. For Fh-DW-NH_4SCN-2 synthesis, the reagents were dissolved in ultrapure water and for Fh-SW-NH_4SCN-2 synthesis in artificial seawater 4.0. Synthesis occurred under the same conditions as in 2.1.2, with only one change: NH_4SCN and KOH were added to the burette and dripped for 1 h into the iron solution. The same amount of NH_4SCN was used as in the 2.1.3 synthesis. After the synthesis, the same treatments were performed as in the 2.1.2. synthesis.

Methods

Infrared spectroscopy

After the samples were lyophilized, the spectra were obtained with a resolution of 4 cm^{-1} in the range 4000 cm^{-1} to 400 cm^{-1}. In total, 16 scans were performed in a Bruker-Vertex 70 spectrometer equipped with an attenuated total reflectance-ATR accessory with a Ge crystal 45°. A small amount of the solid (≈ 10 mg) was added to the crystal

X-Ray Diffraction

The powder samples were analysed by X-ray diffraction using a Shimadzu D6000 diffractometer. CoKα (40 kV, 30 mA) radiation and an iron filter were used in a step-scanning mode (0.02 ° 2θ/0.6 s). All peak positions were analysed using the software Grams 8.0.

Ph at the point of zero charge

The pH at the point of zero charge (pH_{pzc}) is an important parameter as it could be helpful to elucidate whether adsorption involves physical interaction (electrostatic attraction) or chemical interaction (bonding). In 12 tubes of 50 mL with threads, 20 mL of NaCl0.10 mol L^{-1} were added. The pH of each solution was adjusted from 1.00 to12.0 using HCl (0.10 mol L^{-1}) or NaOH (0.10 mol L^{-1}) solutions. Next, 20 mg of iron oxide were added to each tube. The suspensions were stirred for 24 h at room temperature. The samples were centrifuged at 9000 rpm for 10 min and the pH of the samples was measured. A graphic of pH measured versus pH adjusted was made, where the pH_{pzc} corresponding to the pH measured was constant in the range of pH adjusted.

Surface analysis

The surface analysis was performed in High Speed Gas Sorption Analyzer equipment, version 11:02. For determination of pore size, volume and surface area, the methods by Dollimore and Heal (DH) Barret-Joyner Halenda (BJH) Brunauer, Emmett and Teller (BET) were used, respectively. The samples were pretreated at 120 °C under vacuum for 3 h. The measurements were performed at the temperature of liquid N_2 (77.3 K). The results were analysed using the software NovaWin 11.0.

X-ray Photoelectron spectroscopy

X-ray photoelectron spectroscopy (XPS) spectra were collected with an ESCA 3000 spectrometer equipped with conventional

https://doi.org/10.1017/S1473550420000245 Published online by Cambridge University Press

Mg K_α X-ray source and a 250 mm hemispherical energy analyser with an overall resolution of 0.8 eV at an emission angle of 45° and pressures of less than 2×10^{-8} Torr. The adventitious carbon C 1s peak at 285 eV was used as a reference for charge correction. All samples were prepared by spreading a thin layer of the powdered materials on a metallic holder which was air-dried at ~ 100 °C for 2 h and immediately transferred to a UHV chamber. This thermal treatment reduces the amount of water adsorbed in the samples, improving the pressure in the XPS analysis chamber without causing significant changes in the X-ray diffractograms of the samples.

Results and discussion

X-ray diffraction

X-ray diffractograms of Fh-6 and Fh-SW-NH_4SCN-2, and Fh-SW samples presented six characteristic peaks of 6-line ferrihydrite and two characteristic peaks of 2-line ferrihydrite, respectively (Fig. 1) (Cornell and Schwertmann, 2003). Artificial seawater 4.0 Gy only had an effect on the crystallinity of ferrihydrite, since instead of 6-line ferrihydrite, 2-line ferrihydrite was obtained. However, Samulewski *et al.*, observed that in the synthesis of magnetite, besides magnetite, goethite (26.9%) and gypsum (19.4%) were also obtained (Samulewski *et al.*, 2020). The Fh-SW-NH_4SCN-2 sample showed lower crystallinity when compared to the Fh-6 sample, probably due to the high quantity of salts present in seawater 4.0 Gy that interferes with the formation of the ferrihydrite structure. It should be pointed out that ammonium thiocyanate was in the burette along with potassium hydroxide and this solution was dripped into the beaker for 1 h. Thus, for most of the time of the synthesis, the ammonium thiocyanate was at a much lower concentration than the ferrous nitrate or the salts of the artificial seawater 4.0 Gy. Therefore, it probably did not have an effect on the synthesis products, because of its low concentration. Since artificial seawater 4.0 Gy contains a high quantity of Mg^{2+}, there is a possibility that this cation is being incorporated into the ferrihydrite structure, causing crystallinity loss (Giovanoli and Schwertmann, 1992). For the Fh-SW-NH_4SCN-2 sample, the SCN^- anion was added to the burette along with the OH^- anion. Since the SCN^- anion is dripped into the beaker, its concentration is always much lower than the SO_4^{2-} anion concentration. Thus, the SO_4^{2-} anion from artificial seawater interacts with the Fe^{3+} cation forming complexes and the SCN^-anion does not interact with the Fe^{3+} cation (Broadhurst and Preez, 1993).

X-ray diffractograms of Fh-DW-NH_4SCN-2 and Fh-SW-NH_4SCN-1 samples presented characteristic peaks of goethite, hematite and magnetite (Fig. 1). For the Fh-DW-NH_4SCN-1 sample, the X-ray diffractogram presented characteristic peaks of hematite and magnetite (Fig. 1). However, the FT-IR spectra of Fh-DW-NH_4SCN-2, Fh-SW-NH_4SCN-1 and Fh-DW-NH_4SCN-1 samples showed bands at 890 cm^{-1} (O-H bending in plane) and 794 cm^{-1} (O-H bending out of the plane) which are characteristic of goethite (Table 1) (Cornell and Schwertmann, 2003). In addition, Samulewski *et al.* (2020) also observed that when magnetite was synthesized in the presence of SCN^-anion, goethite was also obtained. For Fh-DW-NH_4SCN-1 and Fh-DW-NH_4SCN-2 samples, the (hematite, (018)) and (magnetite, (311)) peaks should be the highest intensity, but probably due to orientation, they are not (Fig. 1). The Fh-6 sample showed weak bands at 890 cm^{-1} and 801 cm^{-1} (Table 1). These bands could be due to the formation of a small amount of goethite, which was not detected by X-ray diffractometry. For the Fh-SW and Fh-SW-NH_4SCN-2 samples these bands were not observed (Table 1).

When thiocyanate was added together with Fe^{3+} (Fh-SW-NH_4SCN-1 and Fh-DW-NH_4SCN-1), at the beginning of the synthesis the concentration of ammonium thiocyanate was high, so the iron oxides showed good crystallinity (Fig. 1). For the sample Fh-DW-NH_4SCN-2, the SCN^- anion was added to the burette along with the OH^- anion, however, unlike the Fh-SW-NH4SCN-2 sample, goethite, magnetite and goethite were obtained (Fig. 1). Probably, in this case, the SCN^- anion is not competing with seawater salts, mainly SO_4^{2-} anion. It should be noted that ferrihydrite has low stability, so ferrihydrite is an intermediate for the synthesis of other iron oxides (Cornell and Schwertmann, 2003).

Pearson's theory

For the synthesis of these materials, Pearson's theory could provide information to the interaction between SCN^- and the Fe^{3+} ion on the formation of the M-SCN or M-NCS bond. The SCN^- ion can bind metals through the sulphur atom or nitrogen atom. When the metal is a hard acid, SCN^- binds through the nitrogen atom and when the metal is a soft acid SCN^- binds through the sulphur atom. Since the Fe^{3+} ion is considered a hard acid, the metal coordinates with the SCN^- ion through nitrogen to form isothiocyanate complexes (Pearson, 1963). It is well known that goethite is formed when sulphur compounds interact with the Fe^{3+} cation (Cornell and Schneider, 1989; Cornell *et al.*, 1989; Cornell and Schwertmann, 2003; Vu and Moreau, 2015; Carneiro *et al.*, 2013; Samulewski *et al.*, 2020). Therefore, this may be an indication that Fe^{3+} interacted with the SCN^- ion also by sulphur. In addition, the formation of magnetite could be an indication that the SCN^- ion oxidized forming thiocyanogen-$(SCN)_2$ or trithiocyanate ion-$(SCN)_3^-$ and the reduction of Fe^{3+} to Fe^{2+} (see reactions below) (Broadhurst and Preez, 1993)

$$2SCN^- + 2Fe^{3+} \Leftrightarrow (SCN)_2 + 2Fe^{2+}$$

$$3SCN^- + 2Fe^{3+} \Leftrightarrow (SCN)_3^- + 2Fe^{2+}$$

Infrared spectroscopy

The main purpose of using infrared spectroscopy was not to confirm the results of X-ray diffractometry but to verify details in the samples that diffractometry would not show. Using infrared spectroscopy, it was possible to verify that some samples have several substances adsorbed on them.

The Fh-DW-NH_4SCN-1, Fh-DW-NH_4SCN-2 and Fh-SW-NH_4SCN-1 samples showed a band at 2050 cm^{-1} due to C≡N stretching of SCN^- (Table 1, online Supplementary Figure S1) (Nakamoto, 1978; Colthup *et al.*, 1990). It should be noted that SCN^- was preconcentrated in all samples where goethite was synthesized (Table 1, Fig. 1). This could be an indication of a mechanism for the preconcentration of SCN^-. In addition, for the goethite formation, sulphur of SCN^- interacts with Fe^{3+} (Cornell and Schneider, 1989; Cornell *et al.*, 1989; Cornell and Schwertmann, 2003; Vu and Moreau, 2005; Carneiro *et al.*, 2013; Samulewski *et al.*, 2020). The

https://doi.org/10.1017/S1473550420000245 Published online by Cambridge University Press

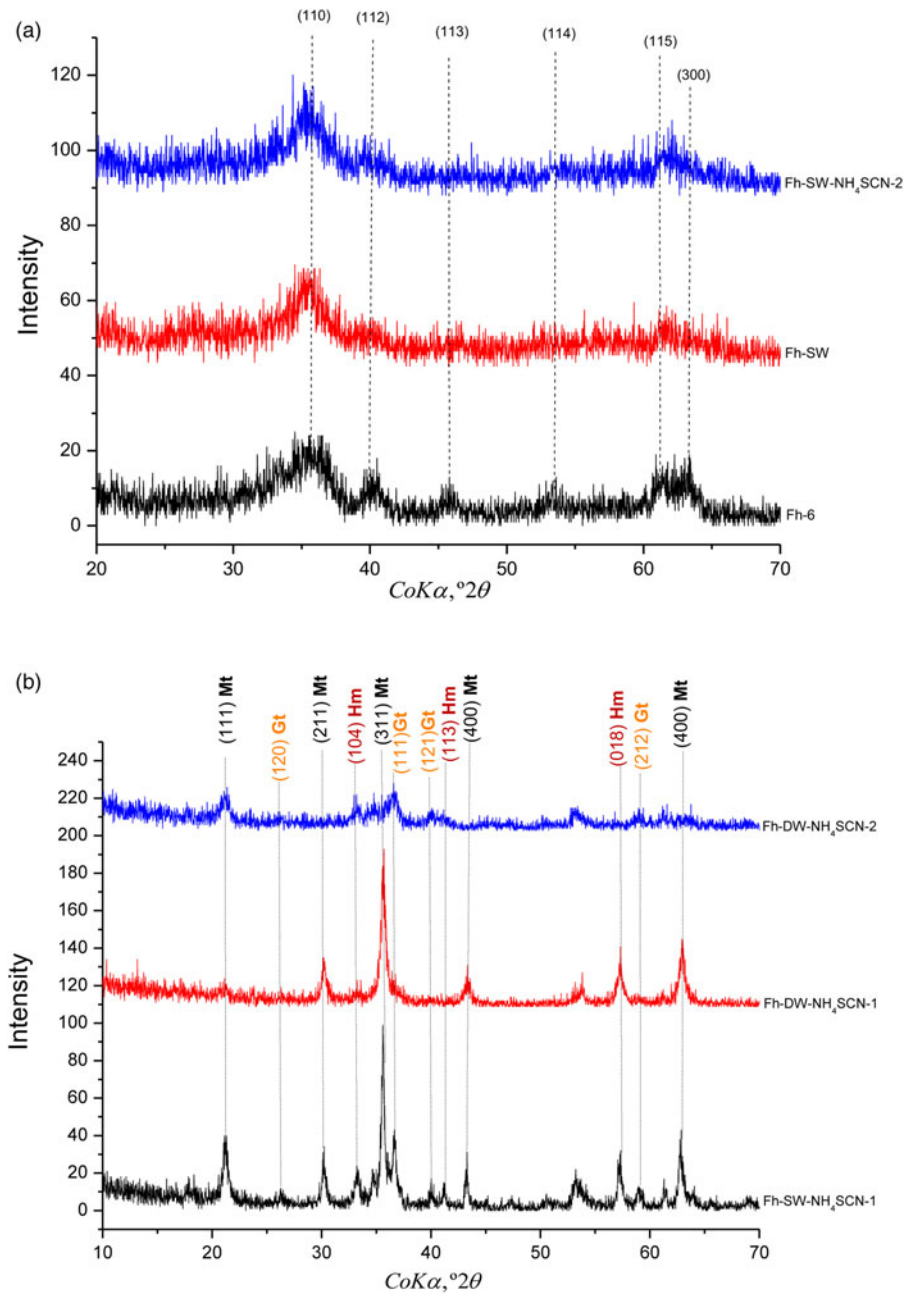

Fig. 1. X-ray diffractograms of the samples (**a**) Fh-6-synthesis of ferrihydrite-6-lines; Fh-SW-4.0-synthesis of ferrihydrite in artificial seawater 4.0 and Fh-SW-NH_4SCN-2-synthesis of ferrihydrite in artificial seawater 4.0 being that NH_4SCN plus KOH together in the burette and (**b**) Fh-SW-4.0-NH_4SCN-1-synthesis of ferrihydrite in artificial seawater 4.0 being that NH_4SCN plus Fe$(NO_3)_3 9H_2O$ together in the beaker; Fh-DW-NH_4 SCN-1-synthesis of ferrihydrite in distilled water being that NH_4SCN plus Fe$(NO_3)_3 9H_2O$ together in the beaker and Fh-DW-NH_4SCN-2-synthesis of ferrihydrite in distilled water being that NH_4SCN plus KOH together in the burette. Mt-magnetite, Hm-hematite, Gt-goethite.

Fh-SW-NH_4SCN-2 sample showed a band at 880 cm^{-1}, which could be an indication of the interaction of SCN^- with Fe^{3+} by nitrogen. However, the band at 2050 cm^{-1} due to C≡N stretching of SCN^- was not observed for this sample (Table 1). The Fh-SW-NH_4SCN-2 sample showed three bands at 2976 cm^{-1}, 2931 cm^{-1} and 2897 cm^{-1} due to N–H stretching of NH_4^+(Table 1, online Supplementary Figure S1) (Nakamoto, 1978; Colthup *et al.*, 1990).

The adsorption of SCN^- anion onto ferrihydrite occurs in a very acidic pH (Vu and Moreau, 2015) or in a neutral pH in the presence of artificial seawater 4.0 Gy, which contains high Mg^{2+}, Ca^{2+} and SO_4^{2-} concentrations (Zaia *et al.*, 2020). It should be noted that the pH of the oceans 4.0 billion years ago was in the range from 6.3 to 7.2 (Halevy and Bachan, 2017; Krissansen-Totton *et al.*, 2018). Thus, the sorption/precipitation of SCN^- and NH_4^+ onto the samples is very important for prebiotic chemistry, as this is a way to preconcentrate these molecules and they could be used for further reactions in molecular evolution.

Fh-SW and Fh-SW-NH_4SCN-2 samples showed bands at 1096 cm^{-1} and 1096/1050 cm^{-1}, respectively (Table 1). These bands are due to S-O stretching from the SO_4^{2-} of the artificial seawater (Nakamoto, 1978; Colthup *et al.*, 1990). These samples (Fh-SW, Fh-SW-NH_4SCN-2) are ferrihydrites (Fig. 1). It should be noted that when SO_4^{2-} interacts with one or more oxygen atoms, the change in symmetry alters the number of vibrational modes. Thus, more bands in the 1097 cm^{-1} region should be observed (Peak *et al.*, 1999; Fukushi *et al.*, 2013; Jonhston and Chrysochoou, 2016). Therefore, the interaction of SO_4^{2-} with the Fh-SW sample is characteristic of an outer-sphere complex and with the Fh-SW-NH_4SCN-2 sample an inner-sphere complex (Peak *et al.*, 1999; Fukushi *et al.*, 2013; Jonhston and Chrysochoou, 2016).

https://doi.org/10.1017/S1473550420000245 Published online by Cambridge University Press

Table 1. Assignments of frequencies (cm^{-1}) in FTIR spectra of the samples

Fh-6 (cm^{-1})	Fh-DW-NH_4SCN-1 (cm^{-1})	Fh-DW-NH_4SCN-2 (cm^{-1})	Fh-SW (cm^{-1})	Fh-SW-NH_4SCN-1 (cm^{-1})	Fh-SW-NH_4SCN-2 (cm^{-1})	Tentative Assignments
				3400-Sh		O-H surface stretching[a]
			3360		3360	O-H stretching[a]
	3327	3327				O-H stretching[a]
3200	3200	3200				O-H stretching[a]
				3145		O-H surface stretching[a]
					2976-w; 2931/2897-vw	N-H stretching[d,e]
	2050	2050-w		2050		C≡N stretching[d,e]
				1785		?
					1648	Adsorbed or lattice water[b,c]
1635	1635	1635	1635	1635		Adsorbed or lattice water[b,c]
1472	1472	1472	1472	1472	1472	Carbonate[b,c]
1345	1345	1345	1345	1345	1345	Carbonate[b,c]
			1096		1096	S-O stretching[d,e]
					1050 (shoulder)	S-O stretching[d,e]
890-w	890	890		895		O-H bending in the plane[a]
					880 (weak)	?
801-w	794	794		794		O-H bending out of the plane[a]
			696/606-Sh		696/606-Sh	Bulk O-H deformation[a]
687	684	684-w				Bulk O-H deformation[a]
	625			625		Fe-O stretching[a]
568						Bulk O-H deformation[a]
450						Fe-O stretching[a]

Sh-shoulder, w-weak, vw-very weak; Fh-6-synthesis of ferrihydrite-6-lines; Fh-DW-NH_4SCN-1-synthesis of ferrihydrite in distilled water being that NH_4SCN plus $Fe(NO_3)_3 9H_2O$ together in the beaker; Fh-DW-NH_4SCN-2-synthesis of ferrihydrite in distilled water being that NH_4SCN plus KOH together in the burette; Fh-SW-4.0-synthesis of ferrihydrite in artificial seawater 4.0; Fh-SW-4.0-NH_4SCN-1-synthesis of ferrihydrite in artificial seawater 4.0 being that NH_4SCN plus $Fe(NO_3)_3 9H_2O$ together in the beaker and Fh-SW-NH_4SCN-2-synthesis of ferrihydrite in artificial seawater 4.0 being that NH_4SCN plus KOH together in the burette.
[a]Cornell and Schwertmann, 2003
[b]Mazzetti and Thistlethwaite, 2002
[c]Ristić *et al.*, 2007
[d]Nakamoto, 1978
[e]Colthup *et al.*, 1990.

For all samples, bands were observed at 1472 cm^{-1} and 1345 cm^{-1} (Table 1, online Supplementary Figure S1). These bands are due to CO_3^{2-} adsorbed onto the samples (Mazzetti and Thistlethwaite, 2002; Ristić *et al.*, 2007). The CO_3^{2-} was from $CO_{2(g)}$ in the air which was absorbed by the synthesis solutions.

Surface analysis

The pore size, volume and surface area are important parameters in material science as well as in prebiotic chemistry, as the material with a high surface area will adsorb more molecules than a low surface area. In addition, pore size is important in prebiotic chemistry because molecules can enter the pores and mimic the walls of a cell. In the pores, the molecules will be protected against UV radiation or hydrolysis and the molecules will be separated from the environment, where reactions could occur (Brasier *et al.*, 2011; Impey *et al.*, 2012). Among the synthesized samples, the Fh-SW sample presented the highest surface area, pore volume and pore size (Table 2). It should be noted that this sample is a 2-line ferrihydrite and showed the lowest crystallinity (Fig. 1). The surface area, pore volume and pore size for the ferrihydrite samples (Fh-6, Fh-SW, Fh-SW-NH_4SCN-2) are close to the values obtained by other studies (Schultz *et al.*, 1987; Stanjek and Weidler, 1992; Cornell and Schwertmann, 2003; Pereira *et al.*, 2019). As the Fh-DW-NH_4SCN-1 and Fh-DW-NH_4SCN-2 samples presented much lower crystallinity than the Fh-SW-NH_4SCN-1 sample (Fig. 1), they showed much higher surface areas than the Fh-SW-NH_4SCN-1 sample (Table 2). It should be noted that these samples are a mixture of magnetite, hematite and goethite (Fig. 1). Fh-SW and Fh-DW-NH_4SCN-2 samples could be classified as mesoporous materials (2 nm −50 nm) and the other

https://doi.org/10.1017/S1473550420000245 Published online by Cambridge University Press

Table 2. Results of adsorption/desorption of N_2 at 77 K in ferrihydrite synthesis (surface analysis BET) and pH_{pzc}

Sample	*BET surface area (m^2 g^{-1})	**BJH pore volume (cm^3 g^{-1})	Pore size (nm)	#pH_{pzc}
Fh-6	200.9	0.148	1.88	8.24
Fh-DW-NH_4SCN-1	214.4	0.780	1.67	6.35
Fh-DW-NH_4SCN-2	219.0	0.332	3.82	6.43
Fh-SW	316.8	0.891	5.89	7.25
Fh-SW-NH_4SCN-1	41.1	0.134	1.68	7.11
Fh-SW-NH_4SCN-2	231.1	0.743	1.68	8.17

*BET Brunauer-Emmett-Teller; **BJH Barrett-Joyner-Halenda; #pH_{pzc} = pH at the Point of Zero Charge Fh-6-synthesis of ferrihydrite-6-lines; Fh-DW-NH_4SCN-1-synthesis of ferrihydrite in distilled water being that NH_4SCN plus $Fe(NO_3)_3 9H_2O$ together in the beaker; Fh-DW-NH_4SCN-2-synthesis of ferrihydrite in distilled water being that NH_4SCN plus KOH together in the burette; Fh-SW-4.0-synthesis of ferrihydrite in artificial seawater 4.0; Fh-SW-4.0-NH_4SCN-1-synthesis of ferrihydrite in artificial seawater 4.0 being that NH_4SCN plus $Fe(NO_3)_3 9H_2O$ together in the beaker and Fh-SW-NH_4SCN-2-synthesis of ferrihydrite in artificial seawater 4.0 being that NH_4SCN plus KOH together in the burette.

samples as microporous materials (< 2 nm) (Table 2) (Cornell and Schwertmann, 2003).

The pH at the point of zero charge

When the pH is above the pH_{PZC}, the material is negatively charged and when it is below this value, the material is positively charged (Parks and de Bruyn, 1962). For prebiotic chemistry, the pH_{PZC} is an important parameter, since, in general, positively charged molecules will preferably adsorb onto negatively charged minerals; the reverse is also true (Lambert, 2008).

The Fh-6 sample contains only ferrihydrite and its pH_{PCZ} was 8.24, which is in accordance with the data obtained in the literature for ferrihydrite, which vary from 7.0 to 8.8 (Kosmulski, 2018). In the case of the Fh-SW sample, which also contains only ferrihydrite (Fig. 1), the pH_{PCZ} was 7.25 (Table 2). This decrease in pH_{PCZ} is probably related to the adsorption of SO_4^{2-} onto the sample (Table 1, 2). Fh-SW-NH_4SCN-2 presented a pH_{PCZ} similar to the Fh-6 sample (Table 2). It should be noted that this sample adsorbed SO_4^{2-} and NH_4^+ (Table 1).

Fh-DW-NH_4SCN-1, Fh-DW-NH_4SCN-, and Fh-SW-NH_4SCN-1 samples contain a mixture of goethite, hematite and magnetite (Table 1, Fig. 1), and their pH_{PCZ} values were 6.35, 6.43 and 7.11, respectively (online Supplementary Figure S3). These values are in the range of pH_{PCZ} for these samples (Cornell and Schwertmann, 2003; Kosmulski, 2018). All these samples adsorbed SCN^-.

X-ray photoelectron spectroscopy

X-ray photoelectron spectroscopy (XPS) is an excellent tool for probing the electronic structures of Fe-O bonds in $Fe_{1-y}O$ (wüstite), α-Fe_2O_3 (hematite), γ-Fe_2O_3 (maghemite), Fe_3O_4 (magnetite) and FeO(OH) (goethite) compounds (Fujii *et al.*, 1999; Yamashita *et al.*, 2008). However, even in the absence of dissolved oxygen, Fe^0 can react with water to form soluble Fe^{2+} and not only iron oxides (Kruger and Calvertm, 1967), but also amorphous black ferric oxyhydroxide (Ding *et al.*, 2000) and ferrihydrite (Fh) (Chernyshova *et al.*, 2007), which is an abundant mineral in the terrestrial crust with an ordered form $Fe_{10}O_{14}(OH)_2 + nH_2O$ where n is close to 1.

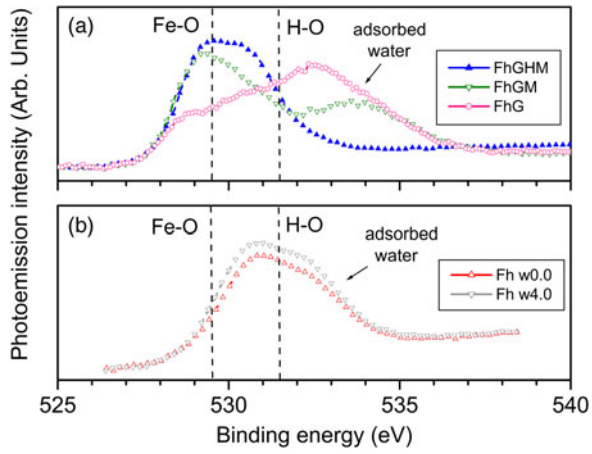

Fig. 2. The XPS spectra of O 1s photopeak from the (a) ferrihydrate mixtured with iron (hidr)oxides compounds and (b) pure ferrihydrate samples.

Fh is a low-crystalline nanoparticulate and highly defective material containing both tetrahedrally and octahedrally coordinated ferric ions (Chernyshova *et al.*, 2010; Michel *et al.*, 2010). Metastable iron oxyhydroxides and particularly maghemite with inverse spinel structure denoted as $(Fe^{3+})_8^{tet}$ $[Fe^{3+}Fe^{2+}]_8^{oct}O_{32}$, where 16 Fe^{3+} and 8 Fe^{2+} occupy tetrahedral (tet) and octahedral (oct) interstitial sites of the oxygen anions, forming a closed-packed FCC lattice and can form Fh by dehydration.

Next, comparisons of the XPS measurements of samples with pure Fh and their mixture with iron oxides are performed. The nomenclature of samples includes the first letter of their constituent compounds as identified by XRD measurements; (*i.e.*), the addition of Gt for goethite, Hm for hematite and Mt for magnetite. Although there is evidence that the binding-energy values of the Fe $2p_{3/2}$ and O 1s peak positions can be dependent on the calibration experimentally obtained from C 1s peak position (Yamashita and Hayes, 2008), we observed systematic changes in O 1s peak position with site occupancy and oxidation state of Fe in the samples containing a mixture of iron oxides and oxyhydroxides.

The XPS O 1s spectra from the samples containing Fh with mixtures of compounds are shown in Fig. 2a, whereas the XPS peaks of O 1s for the pure Fh samples prepared with current seawater (w0.0) and proxy seawater from 4 billion years ago (w4.0) are shown in Fig. 2b.

The contributions Fe-O, H-O and adsorbed water are indicated by dashed lines and arrows in the photopeak region of the O 1s core-level. The peak position of O 1s has been investigated by many works and values between 529 and 532 eV have been reported (Ding *et al.*, 2000; Weiss *et al.*, 2002; Yamashita and P. Hayes, 2008). It is worth noting that the binding energy of the O 1s peak is almost independent of the oxide phase at 530 eV in the presence of both Fe^{3+} and Fe^{2+} species (Schedel-Niedrig *et al.*, 1995; Fujii *et al.*, 1999; Weiss and Ranke, 2002). However, the covalency reduces the number of filled states with O 2p character, so that the strength of the O 1s signal is related to the degree of covalency (Schedel-Niedrig *et al.*, 1995; Weiss and Ranke, 2002). All XPS O 1s spectra shown in Fig. 2a exhibit broad lines at about 529.5 eV, whereas a broader structure with a peak at about 531 eV is observed for pure Fh samples, as shown in Fig. 2b. Furthermore, strong absorption of water is observed in samples containing Fh mixed

https://doi.org/10.1017/S1473550420000245 Published online by Cambridge University Press

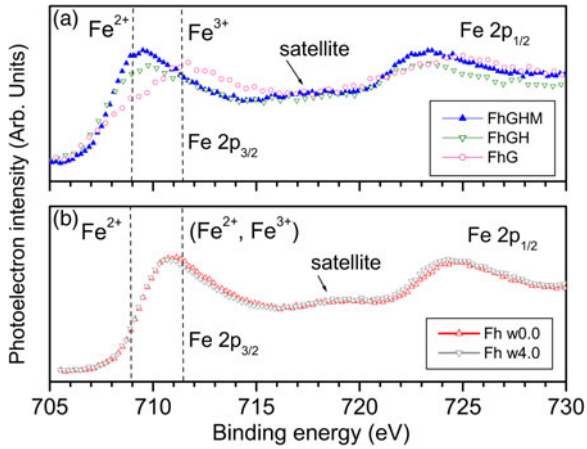

Fig. 3. The XPS spectra of Fe 2p core level from the (a) ferrihydrate mixtured with iron-oxide-based compounds and (b) pure ferrihydrate samples.

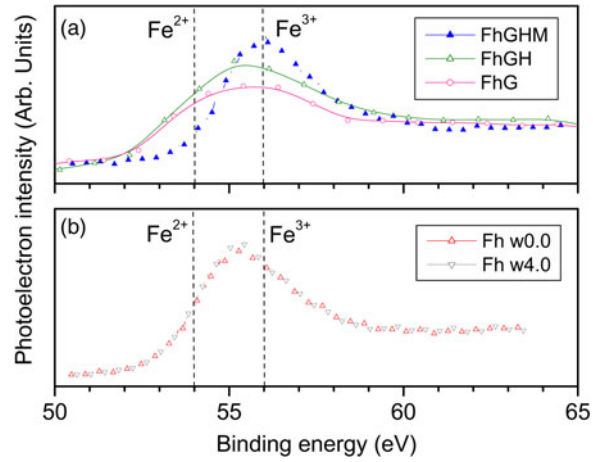

Fig. 4. The XPS spectra of Fe 3p core level from the (a) ferrihydrate mixtured with iron-oxide-based compounds and (b) pure ferrihydrate samples.

with magnetite, hematite and goethite. Particularly, Fh mixed with goethite exhibits a pronounced peak at the position of 533 eV corresponding to water absorption. The water absorption occurs in Fe oxides and a goethite-like phase is reported on the surface of water exposed magnetite samples (Kendelewicz *et al.*, 2000). In hematite, O-H, oxygen-containing carbon species and H_2O surface spectral features are found around 531, 532 and 533 eV, respectively (Yamamoto *et al.*, 2010). The chemisorption of water on the iron oxide surfaces occurs initially on defect sites. No significant changes are observed between samples denoted as Fh w0.0 and Fh w4.0, which exhibit much less adsorbed water after the thermal desorption procedure.

The XPS peaks of Fe $2p_{3/2}$ and Fe $2p_{1/2}$ for the samples containing Fh mixed with iron compounds are shown in Fig. 3a. The peaks Fe $2p_{3/2}$ are narrower and stronger than Fe $2p_{1/2}$ and the area of the Fe $2p_{3/2}$ peak is greater than that of Fe $2p_{1/2}$ because Fe $2p_{3/2}$ has degeneracy of four states while Fe $2p_{1/2}$ has only two from the spin-orbit splitting. The peak position of Fe $2p_{3/2}$ is found at 709 eV for FhGHM and FhGH samples, whereas it appears to be dominated by a component positioned at 711.5 eV for the FhG sample. In addition, these values have been reported by many works (Ding *et al.*, 2000; Yamashita and Hayes, 2008). Whereas the Fe^{2+} species has a spectral component positioned at 709 eV, the Fe^{3+} species in tetrahedral and octahedral sites are positioned between 710.7 and 711.0 eV (Fujii *et al.*, 1999; Weiss and Ranke, 2002; Yamashita and Hayes, 2008). For Fe^{3+}, the Fe $2p_{3/2}$ peak also has an associated shake-up satellite peak which are located approximately 8 eV higher than the main Fe $2p_{3/2}$ peak (Fujii *et al.*, 1999; Weiss and Ranke, 2002; Yamashita and Hayes, 2008).

A particular problem in the case of iron oxides is that Fe_2O_3 can reduce to Fe_3O_4 not only by Ar^+ sputtering but also X-ray exposure in the XPS analysis (Paparazzo, 1986; Lad and Henrich, 1988; Yamashita and Hayes, 2008). Magnetite contains both Fe^{3+} and Fe^{2+} species, which also cause a broader Fe 2p signal than that of the hematite (Weiss and Ranke, 2002), whereas goethite is an iron (oxy)hydroxide containing ferric iron. Clearly, the contribution from (Fe^{2+}, Fe^{3+}) species are predominant in Fh and FhG samples, conforming to Figs. 3a and 3b. The shake-up satellite line characteristic for the Fe^{3+} species at 719 eV binding energy is also visible in XPS spectra of pure Fh samples. The Fe $2p_{3/2}$ signal in the FhG spectrum is asymmetrically broadened, when compared to the FhGHM and FhGH spectra, which can be attributed to excitations of the Fe^{2+} species in the Fh compound. The three Fe-oxides in the FhGHM sample led to a sharper Fe $2p_{3/2}$ profile, indicating a predominance of Fe^{2+} species. Direct comparisons between XPS Fe 2p spectra from Fh w0.0 and Fh w4.0 samples again revealed no significant differences. It is worth noticing that the satellite structures in XPS spectra Fe 2p became unresolved which is likely evidence of the reduction in the Fe_2O_3-Fe_3O_4 system. This was not only due to the formation of Fe^{2+} ions, but also to nonhomogeneous changes in the hybridization parameters between octahedral and tetrahedral Fe^{3+} ions (Fujii *et al.*, 1999).

The XPS spectra of Fe 3p for the samples are shown in Figure4a and 4b. Although the Fe 3p core-level consists of both Fe $3p_{3/2}$ and Fe $3p_{1/2}$, the separation energy of the XPS peaks proportional to the spin–orbit coupling is smaller than the instrumental resolution. Despite the appearance of the Fe 3p peak as a single peak, it is possible to obtain physical parameters from peak position, full width at half maximum (FWHM) and asymmetry of the profile, mainly in Fig. 4a. Peak positions and FWHM of the XPS Fe 3p peak are distinct for samples with Fe only present as Fe^{3+} and Fe^{2+} species (Yamashita and Hayes, 2008). The vertical dashed lines in Fig. 4 indicate the Fe 3p peak positions for Fe^{2+} and Fe^{3+} ions at 54 and 56 eV, respectively.

In Fig. 4a it can be observed that the FWHM and asymmetry of Fe 3p profile for Fe^{2+} are larger than Fe^{3+} for FhG and FhGH samples compared to the FhGHM sample.

Although the Fe 3p peak enables the quantitative analysis of Fe^{3+} and Fe^{2+} using relative areas of each constituent peak assigned to Fe^{2+} and Fe^{3+} without the interference of satellite peaks intervening in Fe 2p peaks, the electronic similarities seen in Fe oxides/oxyhydroxides makes this task complex. Essentially, a certain ubiquity for components arises in the oxide/oxyhydroxide compounds involving essentially close-packed arrangements of oxygen ions, with the Fe ions occupying two kinds of interstitial positions. Excitations of the type $3p^63d^n$ towards $3p^53d^{n+1}$ dominate at the Fe 3p threshold and compete with the direct photoemission process $3p^63d^n$ decaying $3p^63d^{n-1} + e^-$. Nevertheless, the degeneracy of the five Fe 3d states depend on their different orbital overlaps with the O ligands and ligand-field splitting is inversely shifted in octahedral and tetrahedral sites. Thus, the number of unoccupied 3d states available

https://doi.org/10.1017/S1473550420000245 Published online by Cambridge University Press

for mixing with O 2p states (hybridization) is related to either the different local surroundings of the Fe cations and the covalent bonding between Fe 4sp states and O 2p states (Weiss and Ranke, 2002).

Among the reasons why Fe 3p peaks were not used in the present study for the quantitative analysis of the Fe^{2+}/Fe^{3+} ratios in the samples are difficulties in determining linear or Shirley background subtractions, asymmetry factor values and unique Gaussian–Lorentzian ratios in the fitting procedures. High-resolution XPS measurements are required to obtain reliable proportions of iron present in different oxidation states.

Relevance Of this work to prebiotic chemistry

As pointed out in the introduction, NH_4SCN and ferrihydrite could be found on the prebiotic Earth. Of the six most common elements (C, H, O, N, S, P) that make up living beings, NH_4SCN contains four in its composition. Thus, the NH_4SCN/ferrihydrite interaction could be important for prebiotic chemistry. In addition, the composition of the major ions of artificial seawater is close to that of prebiotic Earth (Izawa *et al.*, 2010; Zaia, 2012). There are two important results in this work: (a) the preconcentration of SCN^- and NH_4^+ by sorption/precipitation in the minerals and (b) diversity of iron oxides obtained. There are several ways to preconcentrate biomolecules or precursors of biomolecules: sorption, wetting/drying cycles, freezing/sublimation and natural sorption/precipitation with minerals. In prebiotic chemistry experiments for preconcentration of biomolecules, sorption is the most commonly used method (Zaia, 2004; Lambert, 2008). However, sorption of the SCN^-anion onto several materials occurred only in very acidic pH (Namasivayam and Sureshkumar, 2007; Wu *et al.*, 2011; Vu and Moreau, 2015; Wang *et al.*, 2017). Although a very acidic pH could be found in hydrothermal vents (Holm and Andersson, 2005; Martin *et al.*, 2008), the pH of seawater of prebiotic Earth was close to neutral (Halevy and Bachan, 2017; Krissansen-Totton *et al.*, 2018). In addition, in the synthesis of magnetite in the presence of SCN^- anion, Samulewski *et al.* (2020) did not observe sorption/precipitation of this anion in the synthesized products. Furthermore, the adsorption of SCN^- anion onto magnetite did not occur in a wide pH range (Samulewski *et al.*, 2020). Although ferrihydrite adsorbs SCN^- anion at a neutral pH, high Mg^{2+}, Ca^{2+} and SO_4^{2-} concentrations are necessary (Zaia *et al.*, 2020). Thus, sorption/precipitation of biomolecules with minerals could be an important mechanism for preconcentration of biomolecules or precursors of biomolecules. It should be noted that preconcentration of CO_3^{2-}, SCN^- and NH_4^+ molecules is important for prebiotic chemistry, since they could be used for further reactions in molecular evolution. Since SCN^- anion could have played the same role as CN^- in the Strecker reaction (Perezgasga *et al.*, 2003; Wagner and Ofial, 2015; Kouznetsov and Galvis, 2018), the precipitation/adsorption of thiocyanate by iron oxides is important for prebiotic chemistry. In addition, CO_2 is a source of carbon for the synthesis of several molecules using iron oxides/metal sulphides/clay minerals/zeolites (Schoonen *et al.*, 2004; Holm and Andersson, 2005), thus CO_3^{2-} sorption/precipitation from CO_2 of the atmosphere is also important for the prebiotic chemistry. In addition, a large variety of mineral species could mean much more complex prebiotic chemistry, with more possibilities of catalysts and preconcentrators for the formation of different molecules.

Conclusion

Due to competition between SCN^- and SO_4^{2-} by Fe^{3+}, the way in which SCN^- is added to the reaction medium is probably a determining factor for the formation of iron oxides. Artificial seawater decreased the crystallinity of ferrihydrite synthesized. X-ray diffractograms showed that Fh-DW-NH_4SCN-1, Fh-DW-NH_4SCN-2 and Fh-SW-NH_4SCN-1 samples contain a mixture of goethite, hematite and magnetite. Since goethite was synthesized in these samples, the interaction between Fe^{3+} and SCN^- took place through the sulphur group. In addition, the formation of magnetite is an indication that Fe^{3+} was reduced to Fe^{2+} by SCN^- forming thiocyanogen-$(SCN)_2$ or trithiocyanate ion-$(SCN)_3^-$. FT-IR spectroscopy showed that after the synthesis, SCN^- remains adsorbed onto the Fh-DW-NH_4SCN-1, Fh-DW-NH_4SCN-2 and Fh-SW-NH_4SCN-1 samples, which contain goethite, magnetite and hematite. In addition, NH_4^+ remains adsorbed onto the Fh-SW-NH_4SCN-2 sample after the synthesis. The dragging of these compounds, SCN^- and NH_4^+, during the synthesis is very important for prebiotic chemistry, since this is a way to preconcentrate them for further reactions. It should be pointed out that SCN^- and NH_4^+on the prebiotic Earth may have played important roles in the synthesis of amino acids and nucleic acid bases. In addition, CO_3^{2-} sorption/precipitation by the synthesis products is important for prebiotic chemistry, because CO_3^{2-} was a source of carbon for several syntheses in the primitive Earth. Fh-SW and Fh-SW-NH_4SCN-2 samples adsorbed the SO_4^{2-} anion. The FT-IR spectra showed that SO_4^2 interacts with Fh-SW as an outer-sphere complex and with Fh-SW-NH_4SCN-2 as an inner-sphere complex. Among the ferrihydrites synthesized, the Fh-SW sample presented the highest surface area, the largest pore diameter and lowest crystallinity. Fh-SW and Fh-DW-NH_4SCN-2 samples could be classified as mesoporous materials (2–50 nm) and the other samples as microporous materials (< 2 nm). The pH_{pzc} values of all samples were in the ranges expected.

XPS analyses of the ferrihydrite samples in the presence of iron oxides and oxyhydroxides reveal intricate chemistry associated with the balance of free-valued amounts of Fe^{2+} and Fe^{3+} species, exhibiting variable charge transfer to ligands nearby, together with the preferential choice for the occupation of the tetrahedral and octahedral sites in the oxygen anion lattices. Ferrihydrates prepared with current seawater and proxy 4-billion-years seawater did not show significant differences in the O 1s, Fe 2p and Fe 3p core-level peaks within our experimental resolution. However, possible impacts on (photo)catalytic and biochemical properties of ferric (hydr)oxides cannot be discarded mainly due to the strong effect of water adsorption induced by the presence of (oxy)hydroxides.

Supplementary material. The supplementary material for this article can be found at https://doi.org/10.1017/S1473550420000245

Acknowledgements. The authors thank CNPq/FundaçãoAraucária (Programa de apoio a núcleos de excelência-PRONEX, protocol 24732) and LCNano/UFPR/ Sisnano for their support in this research.

References

Anizelli PR, Baú JPT, Valezi DF, Canton LC, Carneiro CEA, di Mauro E, da Costa ACS, Galante D, Braga AH, Rodrigues F, Coronas J, Casado-Coterillo C, Zaia CTBV and Zaia DAM (2016*a*) Adenine interaction with and adsorption on Fe-ZSM-5 zeolites: a prebiotic chemistry

study using different techniques. *Microporous and Mesoporous Materials* **226**, 493–504.

Anizelli PR, Baú JPT, Gomes FP, da Costa ACS, Carneiro CEA, Zaia CTBV and Zaia DAM (2016*b*) A prebiotic chemistry experiment on the adsorption of nucleic acid bases onto a natural zeolite. *Origins of Life and Evolution of the Biosphere* **45**, 289–306.

Barge LM, Flores E, Baum MM, VanderVelde DG and Russel MJ (2019) Redox and pH gradients drive amino acid synthesis in iron oxyhydroxide mineral systems. *Proceedings of the National Academy of Sciences-USA* **116**, 4828–4833.

Bartlett PD and Davis RE (1958) Reactions of elemental sulfur II. The reaction of alkali cyanides with sulfur and some single sulfur transfer reactions. *Journal of the American Chemical Society* **80**, 2513–2516.

Bassez MP (2018) Water near its supercritical point and at alkaline pH for the production of ferric oxides and silicates in anoxic conditions. A new hypothesis for the synthesis of minerals observed in banded iron formations and for the related geobiotropic chemistry inside fluid inclusions. *Origins of Life and Evolution of the Biosphere* **48**, 289–320.

Bizzarri BM, Botta L, Pérez-Valverde MI, Saladino R, di Mauro E and García-Ruiz JM (2018) Silica metal oxide vesicles catalyze comprehensive prebiotic chemistry. *Chemistry a European Journal* **24**, 8126–8132.

Brasier MD, Matthewman R, McMahon S and Wacey D (2011) Pumice as a remarkable substrate for the origin of life. *Astrobiology* **11**, 725–735.

Braterman PS, Cairns-Smith AG and Sloper RW (1983) Photo oxidation of hydrated Fe^{2+} significance for banded iron formations. *Nature* **303**, 163–164.

Broadhurst JL and du Preez JGH (1993) A thermodynamic study of the dissolution of gold in an acidic aqueous thiocyanate medium using iron (III) sulphate as an oxidant. *Hydrometallurgy* **32**, 317–344.

Canhisares-Filho JE, Carneiro CEA, de Santana H, Urbano A, da Costa ACS, Zaia CTBV and Zaia DAM (2015) Characterization of the adsorption of nucleic acid bases onto ferrihydrite via Fourier transform infrared and surface enhanced Raman spectroscopy and X-ray diffractometry. *Astrobiology* **15**, 728–738.

Carneiro CEA, Berndt G, de Souza Junior IG, de Souza CMD, Paesano Jr A, da Costa ACS, di Mauro E, de Santana H, Zaia CTBV and Zaia DAM (2011) Adsorption of adenine, cytosine, thymine and uracil on sulfide modified montmorillonite: FT-IR, Mössbauer and EPR spectroscopy and X-ray diffractometry studies, *Origins of Life and Evolution of the Biosphere* **41**, 453–468.

Carneiro CEA, Ivashita FF, de Souza Junior IG, de Souza CMD, Paesano Jr. A, da Costa ACS, di Mauro E, de Santana H, Zaia CTBV and Zaia DAM (2013) Synthesis of goethite in solutions of artificial seawater and amino acids: a prebiotic chemistry study. *International Journal of Astrobiology* **12**, 149160.

Carneiro CEA, Stabile AC, Gomes FP, da Costa ACS, Zaia CTB and Zaia DAM (2017) Interaction, at ambient temperature and 80 °C between minerals and artificial seawaters resembling the present ocean composition and that of 4.00 billion years ago. *Origins of Life and Evolution of the Biosphere* **47**, 323–343.

Chernyshova IV, Hochella MF and Madden AS (2007) Size-dependent structural transformations of hematite nanoparticles. 1 phase transition. *Physical Chemistry Chemical Physics* **9**, 1736–1750.

Chernyshova IV, Ponnurangam S and Somasundaran P (2010) On the origin of an unusual dependence of (bio)chemical reactivity of ferric hydroxides on nanoparticle size, *Physical Chemistry Chemical Physics* **12**, 14045–14056.

Colthup NB, Daly LH and Wiberley SE (1990) *Infrared and Raman Spectroscopy*, 3nd Ed. Boston: Academic Press Inc., Harcourt Brace Jovanovich Publishers.

Cornell RM and Schneider W (1989) Formation of goethite from ferrihydrite at physiological pH under the influence of cysteine. *Polyhedron* **8**, 149–155.

Cornell RM and Schwertmann U (2003) *The Iron Oxides: Structure, Properties, Reactions, Occurrences and Uses*. Weinheim: Wiley-VCH Verlag GmbH & Co. KGaA.

Cornell RM, Schneider W and Giovanoli R (1989) Phase transformations in the ferrihydrite/cysteine system. *Polyhedron* **8**, 2829–2836.

Curi R and Procopio J (2017) *Fisiologia Básica*, 2nd Edn. Rio de Janeiro-RJ: Editora Guanabara Koogan Ltda.

Ding M, de Jong BHWS, Roosendaal SJ and Vredenberg A (2000) XPS Studies on the electronic structure of bonding between solid and solutes: adsorption of arsenate, chromate, phosphate, Pb2 + , and Zn2 + ions on amorphous black ferric oxyhydroxide. *Geochimica et Cosmochimica Acta* **64**, 1209–1219.

Dowler MJ and Ingmanson DE (1979) Thiocyanate in Red Sea brine and its implications. *Nature* **279**, 51–52.

Farias APSF, Carneiro CEA, de Batista Fonseca IC, Zaia CTBV and Zaia DAM (2016) The adsorption of amino acids and cátions onto goethite: a prebiotic chemistry experiments. *Amino Acids* **48**, 1401–1412.

Fujii T, de Groot FMF, Sawatzky GA, Voogt FC, Hibma T and Okada K (1999) *In situ* XPS analysis of various iron oxide films grown by NO2-assisted molecular-beam epitaxy. *Physical Review B* **59**, 3195–3202.

Fukushi K, Aoyama K, Yank C, KItadai N and Nakashima S (2013) Surface complexation modeling for sulfate adsorption on ferrihydrite consistent with *in situ* infrared spectroscopic observations. *Applied Geochemistry* **36**, 82–103.

Georgelin T, Akouche M, Jaber M, Sakhno Y, Matheron L, Fournier F, Méthivier C, Martra G and Lambert JF (2017) Iron (III) oxide nanoparticles as catalysts for the formation of linear glycine peptides. *European Journal of Inorganic Chemistry*, 198–211.

Giovanoli R and Schwertmann RM (1992) Crystallization of metal substituted ferrihydrites. *Journal of Plant Nutrition and Soil Science* **155**, 455–460.

Halevy I and Bachan A (2017) The geologic history of seawater pH. *Science (New York, N.Y.)* **355**, 1069–1071.

Halevy I, Alesker M, Schuster EM, Popovitz-Biro R and Feldman Y (2017) A key role for green rust in the precambriam oceans and the genesis of iron formations. *Nature Geoscience* **10**, 135-1–135-5.

Hazen R,M, Papineau D, Bleeker W, Downs RT, Ferry JM, McCoy TJ, Sverjensky DA and Yang H (2008) Mineral evolution. *American Mineralogist* **93**, 1693–1720.

Holm NG and Andersson E (2005) Hydrothermal simulation experiments as a tool for studies of the origin of life on earth and other terrestrial planets: a review. *Astrobiology* **5**, 444–460.

Impey C, Lunine J and Funes J (2012) *Frontiers of Astrobiology*. Cambridge: Cambridge University Press.

Izawa M.R.M, Nesbitt H.W, MacRae N.D and Hoffman E.L (2010) Composition and evolution of the early oceans: Evidence from the Tagish Lake meteorite. *Earth and Planetary Science Letters* **298**(3-4), 443–449. http://dx.doi.org/10.1016/j.epsl.2010.08.026.

Johnston CP and Chrysochoou, M (2016) Mechanisms of chromate, selenate, and sulfate adsorption on Al-substituted ferrihydrite: implications for ferrihydrite surface structure and reactivity. *Environmental Science & Technology* **50**, 3589–3596.

Kasting JF (1987) Theoretical constraints on oxygen and carbon dioxide concentrations in the precambrian atmosphere. *Precambrian Research* **34**, 205–229.

Kasting JF (2009) The primitive earth, chapter 8. In Tze-Fei Wong J and Lazcano A (eds). *Prebiotic Evolution and Astrobiology*. Austin, TX, USA: Landes Bioscience, pp. 57–64.

Kendelewicz T, Liu P, Doyle CS, Brown Jr. GE, Nelson EJ and Chambers SA (2000) Reaction of water with the (100) and (111) surfaces of Fe_3O_4. *Surface Science* **453**, 32–46.

Kosmulski M (2018) The pH dependent surface charging and points of zero charge. VII. Update. *Advances in Colloid and Interface Science* **251**, 115–138.

Kouznetsov VV and Galvis CEP (2018) Strecker Reacton and α-amino nitriles: recent advances in their chemistry, synthesis, and biological properties. *Tetrahedron Letters* **74**, 773–810.

Krissansen-Totton J, Arney GN and Catling DC (2018) Constraining the climate and ocean pH of the early earth with geological carbon cycle model. *Proceedings of the National Academy of Sciences U.S.A.* **115**, 4105–4110.

Kruger J and Calvertm JP (1967) Ellipsometric potentiostatic studies of iron passivity: i anodic film growth in slightly basic solutions. *Journal of The Electrochemical Society* **114**, 43–49.

Lad RJ and Henrich VE (1988) Structure of ∝Fe2O3 single crystal surfaces following Ar + ion bombardment and annealing O_2. *Surface Science* **193**, 81–93.

Lambert J (2008) Adsorption and polymerization of amino acids on mineral surfaces: a review. *Origins of Life and Evolution of the Biosphere* **38**, 211–242.

Liang MC, Hartman H, Kopp RE, Kirschvink JL and Yung YL (2006) Production of hydrogen peroxide in the atmosphere of snow-ball earth and origin of oxygenic photosynthesis. *Proceedings of the National Academy of Science-USA* **103**, 18896–18899.

Martin W, Baross J, Kelley D and Russel MJ (2008) Hydrothermal vents and the origin of life. *Nature Reviews Microbiology* **6**, 805–814. Available at at https://www.nature.com/articles/nrmicro1991.pdf.

Matrajt G and Blanot D (2004) Properties of synthetic ferrihydrite as an amino acid adsorbent and a promoter of peptide bond formation. *Amino Acid* **26**, 153–158.

Mazzetti L and Thistlethwaite PJ (2002) Raman spectra and thermal transformations of ferrihydrite and schwertmannite. *Journal of Raman Spectroscopy* **33**, 104–111.

Michel FM, Barron V, Torrent J, Morales MP, Serna CJ, Boily JF, Liu QS, Ambrosini A, Cismasu AC and Brown GE (2010) Ordered ferrimagnetic form of ferrihydrite reveals links among structure, composition, and magnetism. *Proceedings of the National Academy of Sciences-U. S. A.* **107**, 2787–2792.

Mukhin L (1974) Evolution of organic compounds in volcanic regions. *Nature* **251**, 50–51.

Murad E and Fischer WR (1988) The geobiochemical cycle of iron, chapter 1. In Stucki JW, Goodman B.A., Schwertmann U (eds), *Iron in Soils and Clay Minerals*. Dordrecht, Holland: D. Reidel Publishing Company, pp. 1–18.

Nakamoto K (1978) *Infrared and Raman spectra of Inorganic and Coordination Compounds*. New York: John Wiley & Sons.

Namasivayam C and Sureshkumar D (2007) Modelling thiocyanate adsorption onto surfactant-modified coir pith, an agricultural solid waste. *Trans IChemE, Part B, Process Safety and Environmental Protection* **85**, 521–525.

Paparazzo E (1986) XPS Analysis of iron aluminum oxide systems. *Applied Surface Science* **25**, 1-12.

Parks GA and de Bruyn PL (1962) The zero point of charge of oxides. *The Journal of Physical Chemistry* **66**, 967–973. DOI: doi: 10.1021/j100812a002.

Peak D, Ford RG and Sparks DL (1999) An *in situ* ATR-FTIR investigation of sulfate bonding mechanisms on goethite. *Journal of Colloid and Interface Science* **218**, 289–299.

Pearson G (1963) 'Hard and soft acids and bases. *Journal of the American Chemical Society* **85**, 3533–3539.

Pereira RC, Anizelli PR, di Mauro E, Valezi DF, da Costa CS, Zaia CTBV and Zaia DAM (2019) The effect of pH and ionic strength on the adsorption of glyphosate onto ferrihydrite. *Geochemical Transactions* **20**, 1–14.

Perezgasga L, Silva E, Lazcano A and Negrón-Mendoza A (2003) The sulfocyanic theory on the origin of life: towards a critical reappraisal of naautothrophic theory. *International Journal of Astrobiology* **2**, 301–306.

Raulin F and Toupance G (1977) The role of sulphur in chemical evolution. *Journal of Molecular Evolution* **9**, 329-338.

Ristić M, de Grave E, Musić S, Popović S and Orehovec Z (2007) Transformation of loe crystalline ferrihydrite to α-Fe2O3 in solid state. *Journal of Molecular Structure* **834–836**, 454–460.

Rzepa G, Pieczara G, Gawel A and Tomczyk A (2016) The influence of silicate on transformation pathways of synthetic 2 line ferrihydrite. *Journal of Thermal Analysis and Calorimetry* **125**, 407–421.

Samulewski RB, Gonçalves JM, Urbano A, da Costa ACS, Ivashita FF, Paesano Jr. A and Zaia DAM (2020) Magnetite synthesis in the presence of cyanide or thiocyanate under prebiotic chemistry conditions. *Life Chicago, Ill* **10**, 34-1–34-14.

Savic I, Stojiljkovic S, Savic I and Gajic D (2014) Chapter 15: industrial application of clays and clay minerals. In Wesley LR (ed). *Clays and Clay Minerals: Geological Origin, Mechanical Properties and Industrial Applications*. New York: Nova Publishers, pp. 379–402.

Schedel-Niedrig Th., Weiss W and Schlogl R (1995) Electronic structure of ultrathin ordered iron oxide films grown onto Pt (111). *Physical Review B* **52**, 17449–17460.

Schoonen M, Smirnov A and Cohn C (2004) A perspective on the role of minerals in prebiotic synthesis. *Ambio* **33**, 539–551.

Schultz MF, Benjamin MM and Ferguson JF (1987) Adsorption and desorption of metals on ferrihydrite: reversibility of the reaction and sorption properties of the regenerated solid. *Environmental Science & Technology* **21**, 863–869.

Schwertmann U and Fitzpatrick RW (1992) Iron minerals in surface environments. *Catena Supplement* **21**, 7–30.

Shanker U, Bhushan B, Bhattacharjee and G, Kamaluddin (2011) Formation of nucleobases from formamide in the presence of iron oxides: implication in chemical evolution and origin of life. *Astrobiology* **11**, 225-233.

Shanker U, Bhushan B, Bhattacharjee and G, Kamaluddin (2012) Oligomerization of glycine and alanine catalyzed by iron oxides: implications for prebiotic chemistry. *Origins of Life and Evolution of the Biosphere* **42**, 31-45.

Shanker U, Singh and G, Kamaluddin (2013) Interaction of aromatic amines with iron oxides: implications for prebiotic chemistry. *Origins of Life and Evolution of the Biosphere* **43**, 207-220.

Shaw GH (2016) *Earth's Early Atmosphere and Oceans, and the Origin of Life. Springer Briefs in the Earth Sciences*. Switzerland: Springer International Publishing.

Shinnaka Y, Kawakita H, Jehin E, Decock A, Hutsemékers D, Manfroid J and Arai A (2016) Nitrogen isotopic ratios of NH2 in comets: implications for 15N-fractionation in cometary ammonia. *Monthly Notices of the Royal Astronomical Society* **462**, S195–S209.

Siever R (1992) The silica cycle in the Precambrian. *Geochimica et Cosmochimica Acta* **56**, 3265-3272.

Stanjek H and Weidler PG (1992) The effect of dry heating on the chemistry, surface area, and oxalate solubility of synthetic 2-line and 6-line ferrihydrites. *Clay Minerals* **27**, 397–412.

Stucki JW (2006) Properties and behaviour of iron in clay minerals, chapter 8. In Bergaya F, Theng BKG and Lagaly G (eds). *Handbook of Clay Science*. Amsterdam: Elsevier Science, pp. 423–476.

Summers DP (1999) Sources and sinks for ammonia and nitrite on the early earth and the reaction of nitrite with ammonia. *Origins of Life and Evolution of the Biosphere* **29**, 33–46.

Svobodova H, Kosnáč D, Tanila H, Wagner A, Trnka M, Vitovič P, Hlinkova J, Vavrinsky E, Ehrlich H, Polák Sˇ and Kopani M (2020) Iron–oxide minerals in the human tissues. *Biometals* **33**, 1–13.

Tosca NJ, Jiang CZ, Rasmussen B and Muhling J (2019) Products of the iron cycle on the early earth. *Free Radical Biology and Medicine* **14**, 138–153.

Vieira AP, Berndt G, de Souza Junior IG, di Mauro E, Paesano Jr. A, de Santana H, da Costa ACS, Zaia CTBV and Zaia DAM (2011) Adsorption of cysteine on hematite, magnetite and ferrihydrite: FT-IR, Mössbauer, EPR spectroscopy and X-ray diffractometry studies. *Amino Acids* **40**, 205-214.

Villafañe-Barajas SA, Baú JPT, Colín-García M, Negrón-Mendoza A, Heredia-Barbero A, Pi-Puig T and Zaia DAM (2018) Salinity effects on the adsorption of nucleic acid compounds on Na-montmorillonite: a prebiotic chemistry experiment. *Origins of Life and Evolution of the Biosphere* **48**, 181-200.

Vu HP and Moreau JW (2015) Thiocyanate adsorption on ferrihydrite and its fate during ferrihydrite transformation to hematite and goethite. *Chemosphere* **119**, 987–993.

Wagner A and Ofial AR (2015) Potassium thiocyanate as source of cyanide for the oxidative α-cyanation of tertiary amines. *The Journal of Organic Chemistry* **80**, 2848–2854.

Wang J, Han Y, Li J and Wei J (2017) Selective adsorption of thiocyanate ions using straw supported ion imprinted polymer prepared by surface imprinting combined with RAFT polymerization. *Separation and Purification Technology* **177**, 62–70.

Weiss W and Ranke W (2002) Surface chemistry and catalysis on well-defined epitaxial iron-oxide layers. *Progress in Surface Science* **70**, 1–151.

Weiss W and Ranke W (2002) Surface chemistry and catalysis on well-defined epitaxial iron-oxide layers. *Progress in Surface Science* **70**(1-3), 1–151. http://dx.doi.org/10.1016/S0079-6816(01)00056-9.

Wu T, Sun D, Li Y, Zhang H and Lu F (2011) Thiocyanate removal from aqueous solution by synthetic hydrotalcite sol. *Journal of Colloid and interface Science* **355**, 198–203.

Yamamoto S, Kendelewicz T, Newberg JT, Ketteler G, Starr DE, Mysak ER, Andersson KJ, Ogasawara H, Bluhm H, Salmeron M, Brown Jr. GE and

Nilsson A (2010) Water adsorption on ∝-Fe2O3 (0001) at near conditions. *Journal of Physical Chemistry C* **114**, 2256–2266.

Yamashita T and Hayes P (2008) Analysis of XPS spectra of Fe^{2+} and Fe^{3+} ions in oxide materials. *Applied Surface Science* **254**, 2441–2449.

Yamashita T and Hayes P (2008) Analysis of XPS spectra of Fe2+ and Fe3+ ions in oxide materials. *Applied Surface Science* **254**(8), 2441–2449. http://dx.doi.org/10.1016/j.apsusc.2007.09.063.

Zaia DAM (2004) A review of adsorption of amino acids on minerals: was it important for origin of life? *Amino Acids* **27**, 113–118.

Zaia DAM (2012) Adsorption of amino acids and nucleic acid bases onto minerals: a few suggestions for prebiotic chemistry experiments. *International Journal of Astrobiology* **11**, 229–234.

Zaia DAM, de Carvalho Pereira R and Samulewski RB (2018) Adenine and thymine effect on quartz dissolution at different artificial seawaters. *Orbital: The Electronic Journal of Chemistry* **10**, 446–452.

Zaia DAM, de Carvalho PCG, Samulewski RB, de Carvalho Pereira R and Zaia CTBV (2020) Unexpected thiocyanate adsorption onto ferrihydrite under prebiotic chemistry conditions. *Origins of Life and Evolution of Biospheres* **50**, 57–76.